

## Epitaxial Growth and Erosion on (110) Crystal Surfaces: Structure and Dynamics of Interfacial States

Leonardo Golubović and Artem Levandovsky

*Department of Physics, West Virginia University, Morgantown, West Virginia 26506*

Dorel Moldovan

*Mechanical Engineering Department, Louisiana State University, Baton Rouge, Louisiana 70803-6413*

(Received 5 March 2002; published 10 December 2002)

We study nonequilibrium interfacial states in multilayer epitaxial growth and erosion on rectangular symmetry crystal surfaces. We elucidate a recently observed transition between two kinds of rippled states on (110) surfaces. We predict several novel interface states intervening, via consecutive transitions, between the two rippled states. We predict coarsening laws of the dynamics of the rippled and the intervening states on (110) crystal surfaces.

DOI: 10.1103/PhysRevLett.89.266104

PACS numbers: 68.55.-a, 05.40.-a, 05.70.Ln

Molecular-beam epitaxy growth and erosion of crystal surfaces often manifest striking pyramidal surface structures [1–6]. They are self-assembled nanostructures induced by the classical Ehrlich-Schwoebel-Villain instability [1]. These growing pyramids dominate the crystal interface dynamics, as evidenced in numerous experiments and simulations on high symmetry (100) and (111) crystal surfaces [2–5]. Much less is known about related phenomena on *low symmetry* surfaces. Thus, far from equilibrium interfacial structures in the epitaxial growth and erosion on rather typical *rectangular* symmetry (110) crystal surfaces have attracted attention only recently [7]. Rather than pyramids, rippled (modulated) structures have been observed on (110) surfaces of Fe [8] and Ag [7]. In addition, an intriguing intermediary interface state has been recently revealed in the “ripple rotation” transition between two kinds of rippled states on (110) surfaces [7]. In this Letter, we elucidate the experimental phenomenology of the epitaxial growth and erosion on (110) surfaces. Surprisingly, we find that several novel interfacial states intervene between the rippled states. For the first time, we predict the coarsening laws of the dynamics of common rippled and other states on these simplest low symmetry crystal surfaces.

We base our discussion on the general phenomenological model for multilayer epitaxial growth in the absence of (typically weak) adatom desorption and vacancy creation [1,6],

$$\frac{\partial h}{\partial t} = -\frac{\partial}{\partial x_1} J_1 - \frac{\partial}{\partial x_2} J_2. \quad (1)$$

It expresses the dynamics of the growing surface profile  $h(\mathbf{x}, t)$  in the frame comoving with the interface [ $\mathbf{x} = (x_1, x_2)$ ], as the conservation law involving the surface current  $\mathbf{J} = (J_1, J_2)$  of the form

$$\mathbf{J} = \mathbf{J}^{(\text{NE})}(\mathbf{M}) + \mathbf{J}^{(\text{SD})}. \quad (2)$$

Here,  $\mathbf{J}^{(\text{NE})}$  is the surface nonequilibrium current being

a function of the local interface slope vector  $\mathbf{M} = (M_1, M_2)$ ;  $M_1 = \partial h / \partial x_1$ ,  $M_2 = \partial h / \partial x_2$ .  $\mathbf{J}^{(\text{SD})}$  in Eq. (2) signifies all other curvature currents that vanish on flat interfaces (facets), e.g., the usual surface diffusion current [6]. The (110) surface has rectangular symmetry and the natural coordinate system  $(x_1, x_2)$  with the principal axes along the sides of the surface rectangular unit cell. This symmetry imposes a few ubiquitous properties of  $\mathbf{J}^{(\text{NE})}(\mathbf{M}) = (J_1^{(\text{NE})}(M_1, M_2), J_2^{(\text{NE})}(M_1, M_2))$ . This current vector must transform in the same way the slope vector  $\mathbf{M} = (M_1, M_2)$  transforms under symmetry transformations leaving the rectangle, i.e., the (110) surface invariant. Thus, under the rectangle reflection  $(M_1, M_2) \rightarrow (-M_1, M_2)$ ,  $(J_1^{(\text{NE})}, J_2^{(\text{NE})}) \rightarrow (-J_1^{(\text{NE})}, J_2^{(\text{NE})})$ . Likewise, under the rectangle reflection  $(M_1, M_2) \rightarrow (M_1, -M_2)$ ,  $(J_1^{(\text{NE})}, J_2^{(\text{NE})}) \rightarrow (J_1^{(\text{NE})}, -J_2^{(\text{NE})})$ . On the list of the (110) surface symmetries there is *no* diagonal reflection  $(M_1, M_2) \rightarrow (M_2, M_1)$ , i.e.,  $J_1(M_1, M_2) = J_2(M_2, M_1)$ , present on the square symmetry (100) surfaces [4,5]. Thus, on the rectangular symmetry surfaces, in general,

$$J_1^{(\text{NE})}(M_1, M_2) \neq J_2^{(\text{NE})}(M_2, M_1), \quad (3)$$

simply because the principal axes of the (110) surface are *not* equivalent to each other. Commonly, *stable* zeros of the nonequilibrium current,  $\mathbf{J}^{(\text{NE})}(\mathbf{M}) = \mathbf{0}$ , correspond to the preferred slopes  $\mathbf{M}$  of the facets that develop across the growing interface and organize into large structures, e.g., the square pyramids on (100) surfaces [4,5]. By the rectangular symmetry of (110), there are *three* possible kinds of these preferred slope vectors: (i) *singlet*, for which *both* slope components vanish,  $M_1 = M_2 = 0$ ; (ii) *doublets* of two equivalent (symmetry related) slope vectors, for which *one* of the two components of the slope vector vanishes; there are two *nonequivalent* types of doublets: the pair  $(\pm M_1, 0)$  and the pair  $(0, \pm M_2)$ ; (iii) *quartet* of four equivalent slope vectors, for which *none* of the slope components vanishes:  $(\pm M_1, \pm M_2)$ . In

the unstable epitaxial growth, the singlet at  $\mathbf{M} = \mathbf{0}$  is unstable, and stable facets may thus correspond to the doublets or to the quartet. Thus, the stable doublet  $(\pm M_1, 0)$  gives rise to the structure of alternating facets, with the slopes  $(\pm M_1, 0)$ , comprising the rippled state periodic along the  $x_1$  direction, the  $R_1$  state; see Fig. 1 from the simulations discussed later. Likewise, stable doublet  $(0, \pm M_2)$  gives rise to the rippled state  $R_2$  periodic along the  $x_2$  direction; see Fig. 1. On the other side, the stable quartet  $(\pm M_1, \pm M_2)$  may be expected to give rise to *two-dimensionally* periodic interface structures of four-sided pyramidlike objects, of the form

$$h(x_1, x_2) = M_1|x_1| + M_2|x_2|, \quad (4)$$

within one period (unit cell) of the surface structure,  $|x_1| < \lambda_1/2$  and  $|x_2| < \lambda_2/2$ ; see Fig. 1. By Eq. (4), the contour lines (i.e., step terraces) of these pyramids are *rhombi* (or rhomboids, if roof-top edges develop on the pyramids; see Fig. 1). Thus, we call it the rhomboidal pyramid (RhP) state. By its motif in Eq. (4), the Fourier transform (FT) of this 2D periodic structure,  $\tilde{h}(q_1, q_2)$ , is easily shown to have dominant peaks placed along the  $q_1$  and  $q_2$  axes, at the wave vectors  $[\pm 2\pi(2n+1)/\lambda_1, 0]$  and  $[0, \pm 2\pi(2n+1)/\lambda_2]$ , with the integrated intensities  $I_n \sim (2n+1)^{-4}$ ,  $n = 0, 1, 2, \dots$ . Only these peaks remain at long times when  $\lambda_1, \lambda_2 \gg$  the width of pyramid edges and vertices [as tacitly assumed, for simplicity, in Eq. (4)]. Structurally, the RhP state has the form of a linear superposition of the two rippled states. Our RhP peak pattern corresponds to the intermediary state diffraction data of Ref. [7] revealing the four brightest ( $n = 0$ ) among our peaks, at the wave vectors  $[\pm 2\pi/\lambda_1, 0]$  and  $[0, \pm 2\pi/\lambda_2]$ . Such a four-lobe diffraction pattern is manifest in the RhP FT magnitude plot in Fig. 1 from our simulations (all other peaks are smeared by the positional disorder of the pyramid lattice). This and the fact that our RhP state indeed intervenes between the two rippled phases in our phase diagram in Fig. 1 (detailed hereafter) qualify the RhP to be the novel interfacial state inferred from the experiments on Ag(110) [7]. Is the RhP state the only one qualifying for this?

To answer this, we expose the phenomenology of the epitaxial growth and erosion on (110) surfaces, by considering the dynamical model Eq. (1) with generic form on the nonequilibrium current  $\mathbf{J}^{(\text{NE})}(\mathbf{M})$ . It can be obtained as an expansion in powers of  $\mathbf{M}$  respecting stringent restrictions imposed by the rectangular symmetry. By the inversion symmetry of (110), this expansion must contain only odd powers of  $\mathbf{M}$ . By respecting the rectangle reflection symmetries, we arrive at the general expansion of the form

$$\begin{aligned} J_1^{(\text{NE})} &= M_1[r_1 - u_{11}M_1^2 - u_{12}M_2^2 + \dots], \\ J_2^{(\text{NE})} &= M_2[r_2 - u_{21}M_1^2 - u_{22}M_2^2 + \dots]. \end{aligned} \quad (5)$$

Because of the rectangular anisotropy Eq. (3),  $r_1 \neq r_2$ ,

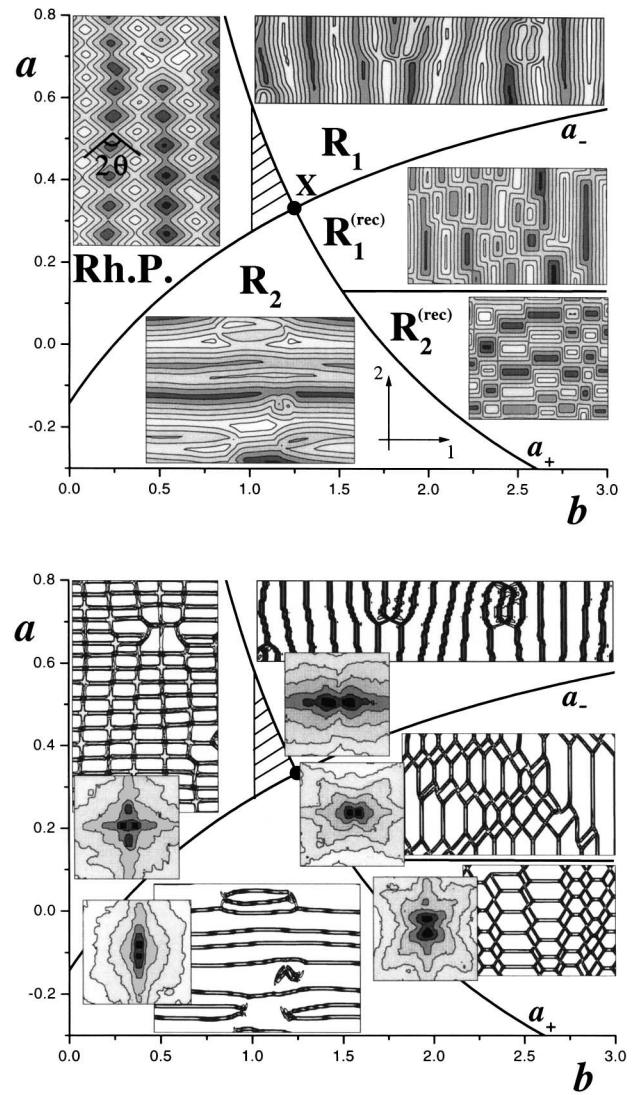


FIG. 1. The phase diagram of the interface model with  $\mathbf{J}^{(\text{NE})}(\mathbf{M})$  in Eq. (5). It depends on only *three* dimensionless parameters:  $a = (r_1/\sqrt{u_{11}} - r_2/\sqrt{u_{22}})/(r_1/\sqrt{u_{11}} + r_2/\sqrt{u_{22}})$ ,  $b = (u_{12} + u_{21})/2\sqrt{u_{11}u_{22}}$ , and  $c = (u_{12} - u_{21})/2\sqrt{u_{11}u_{22}}$ . We depict it in the  $(b, a)$  plane for a fixed  $c$  (here  $c = 3/4$ ). Upper panel: interface contour plots from our simulations. Lower panel: the corresponding networks of facet edges and FT, i.e., diffraction patterns of various interface states: the rhomboidal pyramid (RhP), two ordinary rippled  $R_1$  and  $R_2$ , and two rippled rectangular states  $R_1^{(\text{rec})}$  and  $R_2^{(\text{rec})}$ . Buckled rippled  $R^{(\text{buc})}$  state is in the hatched area, between the line  $b = 1$  and the  $X$  point at  $b = \sqrt{1 + c^2}$ ,  $a = (\sqrt{1 + c^2} - 1)/c$ , at the intersection of the two lines  $a = a_+ = (1 - b + c)/(1 + b - c)$  and  $a_- = -(1 - b - c)/(1 + b + c)$ , marking state boundaries.  $\theta$  is the rhomboidal angle of the RhP state pyramids:  $\tan(\theta) \sim \sqrt{(a_+ - a)/(a - a_-)}$ . The transition between  $R_1^{(\text{rec})}$  and  $R_2^{(\text{rec})}$  is along the horizontal line at  $a = a_{\text{cr}} = [\sqrt{1 + (c/3)^2} - 1]/(c/3)$ . The FT of the  $R^{(\text{rec})}$  states are peak quartets  $(\pm q_1, \pm q_2)$  which, at long times, degenerate into the peak doublet  $(\pm q_1, 0)$  for the  $R_1^{(\text{rec})}$ , or into the peak doublet  $(0, \pm q_2)$  for the  $R_2^{(\text{rec})}$  (as  $\lambda/\xi \rightarrow 0$ ; see the text).

$u_{11} \neq u_{22}$ , and  $u_{12} \neq u_{21}$ , in general. The simplest, basic growth model is naturally obtained by truncating out the higher order terms in the ellipses in Eq. (5), by considering typical situations with small selected slopes. In this limit, one is led to model  $\mathbf{J}^{(\text{SD})}$  terms in Eq. (2) by the anisotropic (rectangularly asymmetric) version of the standard surface diffusion current [9]. Such a minimal model exhibits a number of interfacial states generic for (110) crystal surfaces, as documented in its (far-from-equilibrium) phase diagram in Fig. 1. It is deduced by linear stability analysis of the facets corresponding to the zeros of  $\mathbf{J}^{(\text{NE})}(\mathbf{M})$  in Eq. (5), and further corroborated by numerical simulations of the model in Eqs. (1), (2), and (5). In Fig. 1, we see the standard rippled phases  $R_1$  and  $R_2$ , emerging due to doublets at slopes  $(\pm \sqrt{r_1/u_{11}}, 0)$  and  $(0, \pm \sqrt{r_2/u_{22}})$ , respectively. In Fig. 1, we see also the rhomboidal pyramid RhP state, emerging due to the quartet of four equivalent facets  $(\pm M_1, \pm M_2)$ , with  $M_1$  and  $M_2$  vanishing *both* square brackets in Eq. (5). The quartet facets are stable only in the indicated RhP region in Fig. 1. Therein,  $R_1$  and  $R_2$  doublets are both unstable, leaving the RhP as the selected interface state at long times; see Fig. 1. The ripple rotation phenomena seen on Ag(110) here correspond to the sequence of two consecutive bifurcation transitions: at one of them (along the  $a_+$  line in Fig. 1), RhP continuously transforms into  $R_1$  ( $M_2 \rightarrow 0, M_1 \rightarrow \pm \sqrt{r_1/u_{11}}$ ), whereas at the other bifurcation (along the  $a_-$  line in Fig. 1), RhP continuously transforms into  $R_2$  ( $M_1 \rightarrow 0, M_2 \rightarrow \pm \sqrt{r_2/u_{22}}$ ). In between the two transitions, one has the stable RhP state, which is an anisotropic version of one of the two familiar square pyramid states on (100) surfaces (the phase I [4]), with pyramid edges along principal axes of the surface, as in Fig. 1. The RhP state, with a rectangular network of edges in Fig. 1, coarsens much like the square pyramid phase I (with the square network of edges), by the motion and annihilations of the dislocations of the pyramids edges network [4]; e.g., the interface width  $w \sim t^\beta$ , with  $\beta \approx 1/4$ , away from the transitions to other interface states in Fig. 1. However, a substantially faster coarsening, with  $\beta \approx 0.32$  we find in the RhP region close to the  $R^{(\text{buc})}$  state (hatched region in Fig. 1) discussed later on. Such an enhanced coarsening of the intermediary state (faster than that of nearby rippled states, see below) has been observed also in the experiments [7]. The coarsening of the common rippled states  $R_1$  and  $R_2$  is also mediated by moving dislocations destroying perfect periodicity of these states (see the ripple edged plots in Fig. 1). They are strikingly similar to the dislocations of 2D smectics A [10]. In addition to the interface width  $w$  and the average ripple period  $\lambda$ , the rippled states are characterized by the *coherence length* of ripples,  $\xi$ , corresponding to the separation between dislocations along a ripple (see Fig. 1). Both  $\lambda(t)$  and  $\xi(t)$  are extracted from the anisotropic correlation function  $\langle h(x_1, x_2, t)h(0, 0, t) \rangle = w(t) \psi(x_1/\lambda(t), x_2/\xi(t))$  for the  $R_1$  phase, with  $\psi$  decaying in an oscil-

latory fashion along  $x_1$  and monotonously along  $x_2$ . Away from the transitions to other states in Fig. 1,  $w \sim \lambda \sim t^{n_\lambda}$ , with  $n_\lambda \approx 0.28$ , and  $\xi \sim t^{n_\xi}$ , with  $n_\xi \approx 0.56$ , suggesting the scaling relation  $n_\xi = 2n_\lambda$  [4].

In addition to passing through the RhP and the  $R^{(\text{buc})}$  states, transitions between simple rippled states  $R_1$  to  $R_2$  may also go through the structures called rectangular rippled states,  $R_1^{(\text{rec})}$  and  $R_2^{(\text{rec})}$  (in Fig. 1). Within the range of these  $R^{(\text{rec})}$  states, the two *nonequivalent* doublets  $(\pm M_1, 0)$  and  $(0, \pm M_2)$ , giving rise to the facets of  $R_1$  and  $R_2$ , are *both* locally stable. These facets comprise the basic motif of the two  $R^{(\text{rec})}$  states, that is a rooflike pyramid with a *rectangular* base  $\lambda \times \xi$ , yielding rectangular contour lines in Fig. 1. The base sizes  $\lambda$  and  $\xi$  are along the two (nonequivalent) principal directions of the (110) surface. We find them grown with *different* power laws:  $\lambda \sim t^{n_\lambda}$ ,  $n_\lambda \approx 0.25$ ;  $\xi \sim t^{n_\xi}$ ,  $n_\xi \approx 0.50$ . As  $w(t) \sim \lambda(t) \ll \xi(t)$  at long times, such rectangular pyramid states are a special kind of rippled states with the period  $\lambda(t)$ , as evidenced also by their diffraction patterns; see Fig. 1. The scale  $\xi(t)$  is essentially the length of long roof-top edges present on these rooflike pyramids; see Fig. 1. These edges develop and grow either along the  $x_2$  direction in the  $R_1^{(\text{rec})}$ , or along the  $x_1$  direction in the  $R_2^{(\text{rec})}$  state. These roof-top edges do not develop only along the transition line between  $R_1^{(\text{rec})}$  and  $R_2^{(\text{rec})}$  states in Fig. 1. Along this transition line, the (110) surface develops a state with a simple rhomboidal network of edges that is an anisotropic version of the square pyramid phase II on (100) surfaces [4] [with pyramid facets slope vectors along the equivalent principal axes of the (110) surface, and square networks of edges along the diagonals]. This line is a far-from-equilibrium first-order-like transition at which the two nonequivalent doublets of (110) surfaces, giving rise to  $R_1$  and  $R_2$  states, can coexist. This Gibbs-like coexistence requires the existence of the stationary solution ( $\partial h/\partial t = 0$ ) of Eq. (1) being the interface (edge) between *infinite*  $R_1$  and  $R_2$  facets. This requirement yields an analytic prediction for the position of the  $R_1^{(\text{rec})}$  to  $R_2^{(\text{rec})}$  transition line (see Fig. 1 caption) that is corroborated by our simulations in Fig. 1. In this scenario, the ripple “rotation” transition occurs at a sharp, critical value of a system control parameter (e.g., temperature). This is unlike what is seen on Ag(110), with intervening states such as the RhP and  $R^{(\text{buc})}$  as in our Fig. 1.

Our model exhibits one more state, the aforementioned buckled rippled ( $R^{(\text{buc})}$ ) state that borrows the corner region from the RhP state (hatched region in Fig. 1). Therein, strikingly, *all* zeros of  $\mathbf{J}^{(\text{NE})}(\mathbf{M})$  are *unstable* (in contrast to the rest of the phase diagram, with at least some zeros stable). This can never happen for interfaces in which the dynamics is governed by a free energy or by an effective free energy [4] that actually exists for our model in Eq. (5), *only* for the special case  $u_{12} = u_{21}$  [11]. However, as noted below Eq. (5), in *general*,  $u_{12} \neq u_{21}$  for (110) surfaces. Thus, the unusual region with all zeros

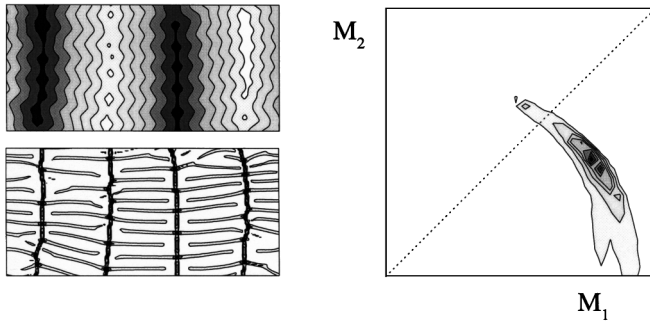


FIG. 2.  $R^{(\text{buc})}$  state, with the contour plots of  $P(M_1, M_2)$  in the  $M_1 > 0, M_2 > 0$  domain. The quartet zero of  $\mathbf{J}^{(\text{NE})}(\mathbf{M})$  is set here on the line  $M_1 = M_2$ . Notably, the preferred  $\mathbf{M}$  is *off* the quartet zero position.

of  $\mathbf{J}^{(\text{NE})}(\mathbf{M})$  unstable is generic for (110) surfaces. Its very existence escapes the common wisdom that stable facets with vanishing  $\mathbf{J}^{(\text{NE})}(\mathbf{M})$  dominate the epitaxial growth with slope selection (as no facet is stable here): In the region of our  $R^{(\text{buc})}$  state in Fig. 1, after a long transient involving ordering of pyramidal chains, the interface eventually selects the shape of a rippled phase with buckled ripples, structurally similar to the RhP state; see Fig. 2.  $R^{(\text{buc})}$  has a motif similar to that of RhP, Eq. (4), however, with  $M_1$  and  $M_2$  therein *not* corresponding to a zero of  $\mathbf{J}^{(\text{NE})}(\mathbf{M})$ . Structurally, and according to its position in the phase diagram in Fig. 1, the  $R^{(\text{buc})}$  state may also qualify to be the state intervening between  $R_1$  and  $R_2$  states seen on the Ag(110) surface. Strikingly, in contrast to the RhP and all other states here, the facets of the  $R^{(\text{buc})}$  state do not assume slopes that vanish  $\mathbf{J}^{(\text{NE})}(\mathbf{M})$ . Rather, these facets carry nonvanishing, *persistent* downhill surface currents Eq. (2), going horizontally in Fig. 2. Their current flux is compensated by uphill currents in the horizontal faint edges in Fig. 2. The distribution of interface slope vectors  $P(M_1, M_2, t)$  approaches a stable form peaked *off* the zeros of  $\mathbf{J}^{(\text{NE})}(\mathbf{M})$ ; see Fig. 2. Thus, the uncommon  $R^{(\text{buc})}$  state *does* exhibit the slope selection although there are no stable zeros of  $\mathbf{J}^{(\text{NE})}(\mathbf{M})$ . We find  $R^{(\text{buc})}$  to exhibit a fast coarsening: the interface width  $w \sim t^\beta$ , with  $\beta \approx 0.40$  close to the center of the  $R^{(\text{buc})}$  range in Fig. 1. This fast coarsening can be used to distinguish the  $R^{(\text{buc})}$  from the RhP state in experiments.

In summary, the epitaxial growth and erosion of (110) surfaces are shown to *generically* exhibit interesting interfacial states intervening between simple rippled states. Two of them, the rhomboidal pyramid state and the unusual buckled rippled state, structurally and according to their position in the phase diagram, qualify to be the

novel interface state recently seen on Ag(110). For the intervening states and for the common rippled states, we have predicted the interface coarsening laws yet to be studied in experiments.

L. G. thanks the DAAD for Grant No. A/02/15054, and M. Biehl, who noted applicability of our phenomenology also to the rectangularly reconstructed (100) surfaces of GaAs and CdTe.

- [1] J. Villain, J. Phys. I (France) **1**, 19 (1991).
- [2] T. Michely *et al.*, Phys. Rev. Lett. **86**, 2859 (2001), and references therein.
- [3] J. Amar, Phys. Rev. B **60**, R11 317 (1999).
- [4] D. Moldovan and L. Golubovic, Phys. Rev. E **61**, 6190 (2000).
- [5] M. Siegert, Phys. Rev. Lett. **81**, 5481 (1998).
- [6] J. Krug, Adv. Phys. **46**, 139 (1997).
- [7] See F. B. de Mongeot *et al.*, Phys. Rev. Lett. **84**, 2446 (2000); see Ag(110) growth simulations in F. Hontinfinde and R. Ferrando, Phys. Rev. B **63**, R121403 (2001), well below the reconstruction and roughening temperatures of Ag(110). Initially suggested intermediary state structure, the regular checkerboard of rectangular mounds has FT with four equivalent dominant peaks at  $(\pm q_1, \pm q_2)$ , and it is *inconsistent* with the diffraction data of de Mongeot *et al.*, having the four peaks at  $(\pm q_1, 0)$  and  $(0, \pm q_2)$ , i.e., the RhP pattern in our Fig. 1. The pyramidal structures seen in the scanning tunneling microscopy (STM) images of G. Constantini *et al.*, J. Phys. Condens. Matter **13**, 5875 (2001), of epitaxial erosion on *both* Ag(100) and Ag(110) [see their Figs. 6(b) and 4], are like those of Refs. [4,5], with both mountains and pits present. These STM images qualitatively differ from those from the simulations of Ag(100) growth [K. J. Casperson *et al.*, Phys. Rev. B **65**, 193407 (2002)] in which the vertical asymmetry completely suppresses the pits. Moreover, such a no-pit state on (110) yields the dominant peaks at  $(\pm q_1, \pm q_2)$ , i.e., has a diffraction pattern different from that observed in Ag(110) growth. Thus, the vertical asymmetry most likely plays a secondary role in both the growth and the erosion on Ag(110).
- [8] M. Albrecht *et al.*, Surf. Sci. **294**, 1 (1993).
- [9] Such  $\mathbf{J}^{(\text{SD})}$  contributes to the interface velocity in Eq. (1) the term  $-\kappa_{11}\partial_1^4 h - 2\kappa_{12}\partial_1^2\partial_2^2 h - \kappa_{22}\partial_2^4 h$ . The values of  $\kappa_{ij}$  do not affect our stability phase diagram: Stability of facets depends only on the parameters of  $\mathbf{J}^{(\text{NE})}$  in Eq. (5).
- [10] J. Toner and D. R. Nelson, Phys. Rev. B **23**, 316 (1981).
- [11] Only for  $u_{12} = u_{21}$ ,  $\mathbf{J}^{(\text{NE})}(\mathbf{M}) = -\partial U(\mathbf{M})/\partial \mathbf{M}$ , with  $U(\mathbf{M}) = u_{11}M_1^4/4 + u_{12}M_1^2M_2^2/2 + u_{22}M_2^4/4$ . The existence of  $U(\mathbf{M})$  excludes the situations with all zeros of  $\mathbf{J}^{(\text{NE})}(\mathbf{M})$  unstable. Thus, the  $R^{(\text{buc})}$  disappears for  $u_{12} = u_{21}$ , i.e.,  $c = 0$  (see Fig. 1 caption).